High salt solution structure of a left-handed RNA double helix

Mariusz Popenda, Jan Milecki[1] and Ryszard W. Adamiak*

Laboratory of Structural Chemistry of Nucleic Acids, Institute of Bioorganic Chemistry, Polish Academy of Sciences, Noskowskiego 12-14, 61-704 Poznań, Poland and [1]Faculty of Chemistry, Adam Mickiewicz University, Poznań, Poland

PDB ID 1T4X

ABSTRACT

Right-handed RNA duplexes of $(CG)_n$ sequence undergo salt-induced helicity reversal, forming left-handed RNA double helices (Z-RNA). In contrast to the thoroughly studied Z-DNA, no Z-RNA structure of natural origin is known. Here we report the NMR structure of a half-turn, left-handed RNA helix $(CGCGCG)_2$ determined in 6 M $NaClO_4$. This is the first nucleic acid motif determined at such high salt. Sequential assignments of non-exchangeable proton resonances of the Z-form were based on the hitherto unreported NOE connectivity path $[H6_{(n)}$-$H5'/H5''_{(n)}$-$H8_{(n+1)}$-$H1'_{(n+1)}$-$H6_{(n+2)}]$ found for left-handed helices. Z-RNA structure shows several conformational features significantly different from Z-DNA. Intra-strand but no inter-strand base stacking was observed for both CpG and GpC steps. Helical twist angles for CpG steps have small positive values (4–$7°$), whereas GpC steps have large negative values ($-61°$). In the full-turn model of Z-RNA (12.4 bp per turn), base pairs are much closer to the helix axis than in Z-DNA, thus both the very deep, narrow minor groove with buried cytidine 2′-OH groups, and the major groove are well defined. The 2′-OH group of cytidines plays a crucial role in the Z-RNA structure and its formation; 2′-O-methylation of cytidine, but not of guanosine residues prohibits *A to Z* helicity reversal.

INTRODUCTION

Right-handed double-helical DNA and RNA have one of the most intriguing structural features in common—the inversion of the helical screw sense, the phenomenon often called helicity reversal or helical transition. Following the discovery of a left-handed double-helical Z-DNA form of $d(CGCGCG)_2$ in the crystal state (1), a similar tendency of RNA double helices i.e. poly(CG) (2) and short duplexes like $(CGCGCG)_2$ (3) to form left-handed Z-RNA was reported. The propensity of right-handed double strands to undergo the *A to Z* transition is most characteristic of RNA containing alternating CG base pairs (4–6). The left-handed RNA prevails at much higher salt concentration, e.g. 6 M $NaClO_4$ (2,3), than that noted for $d(CG)_n$ Z-form duplexes (2.6 M NaCl) (7).

Despite the collection of physical, chemical and spectral data on structural and environmental factors promoting the *A to Z* transition (2,3,8,9), no detailed structure of a left-handed RNA helix of natural sequence has been known to date. This is in great contrast to the abundance of data on the Z-DNA structure. Owing to the excellent crystallization properties of some Z-helix-forming DNA duplexes we have now access to nearly 60 X-ray structures of Z-DNA. There are only two known NMR structures of $d(CG)_n$ duplexes (10,11), however, both contain an 8-methyl-deoxyguanosine residue which, due to its prompt manifestation of the *syn* conformation, promotes Z-DNA formation under very low salt conditions (below 200 mM NaCl).

In the mid 1980s, short oligoribonucleotide duplexes containing either 8-methyl- or 8-bromoguanosine residues were studied in order to forecast the Z-RNA structure (12–14). A preliminary report (14) on the 1.2 Å X-ray study of a tetramer duplex $[C(Br^8G)]_2$ crystallized in the left-handed form under low salt conditions pointed to an intra-strand hydrogen bond formation between the 2′-OH group of cytidine residues and the N3 of the adjacent guanine base on the 5′ side. The hydrogen bonding of the same 2′-OH group, although directed to the guanine *exo*-amino function, was observed in the central part of the crystal structure of a chimeric $[d(CG)r(CG)d(CG)]_2$ (15) and in the Z-RNA model of $(CGCGCG)_2$ generated via energy minimization using Z-DNA coordinates (16). Our knowledge of structural features of Z-RNA in solution is based on the early NMR study of $(CGCGCG)_2$ in high salt (17). Spectra containing both Z- and A-forms were resolved and analysed taking advantage of the slow kinetics of the *A to Z* transition in 6 M $NaClO_4$. In the left-handed form of $(CGCGCG)_2$, cytidine residues in the *anti* conformation adopt an unusual for RNA, C2′-*endo* sugar pucker while guanosine residues preserve the C3′-*endo* sugar pucker but show the *syn* conformation—the landmark of Z-helices. Only a part of the Z-RNA duplex corresponding to its single strand was reported at that time (17).

In contrast to the Z-DNA that has been observed *in vivo*, stabilized by negative supercoiling of the DNA upstream of the moving RNA polymerase (18,19), the biological role of Z-RNA has long been in question due to the non-physiological conditions necessary to accomplish the formation of Z-RNA tracts. This controversy, despite the report on the antibody-aided visualization of Z-RNA tracts in ribosomal RNA (20), has strongly inhibited the development in the area of Z-RNA research and made it dormant over a decade. A report on the induction and stabilization of the $(CG)_6$ in the left-handed form by the RNA-editing enzyme human dsRNA adenosine deaminase (ADAR1) (21,22), a member of the growing family of Z-DNA binding proteins (23,24) prompted us to determine the Z-RNA helix structure. It may be noted that the absence of a Z-RNA structure forced the authors (21,22) to use Z-DNA coordinates to mimic Z-RNA when modelling the Z-RNA/ ADAR1 complex.

Here, we report the NMR structure of a short, left-handed RNA helix $(CGCGCG)_2$ determined in 6 M $NaClO_4$. This is the first nucleic acid motif determined at such high salt. During structure determination, a sequential assignment of non-exchangeable proton resonances of the Z-RNA was based on a hitherto unreported NOE connectivity path for left-handed helices. The Z-RNA helix shows several conformational features significantly different from Z-DNA, e.g. a unique stacking, alternating, low positive and high negative helical twist angle values, a small helical rise and base pairs location close to the helix axis. Both helix grooves of Z-RNA are well defined. Cytidine 2′-OH groups, deeply buried in the narrow minor groove, play a crucial role in the Z-RNA structure and *A to Z* helicity reversal. We hope that our results will be of general interest for those investigating RNA structures and helpful in the studies of structural events in the RNA replication machinery. The Z-RNA structure would also be of particular interest for the studies of interactions of left-handed helices with proteins containing the $Z\alpha$ domain.

MATERIALS AND METHODS

Oligoribonucleotide samples

Hexamer duplexes: $(CGCGCG)_2$, 2′-O-Me$(CGCGCG)_2$ and selectively 2′-O-methylated $[C(2'-OMe)G]_3$ and $[(2'-OMeC)G]_3$ were prepared by automated solid-phase synthesis using 2′-O-tBDMSi-protected (25,26) and 2′-O-methylated (27) ribonucleoside phoshoramidites. Oligoribonucleotides were speed vacuum dried from D_2O (99.8%) three times, dissolved in D_2O (99.98%) buffer containing 150 mM NaCl, 10 mM sodium phosphate pH 6.5, 0.1 mM EDTA and then dried and dissolved in the D_2O (99.98%, 0.6 ml). To measure spectra at higher salt concentration (0.5–6 M $NaClO_4$), dry, crystalline $NaClO_4$ was added to the NMR tube and the resulting solution concentrated using argon flow. Final RNA concentrations were in the range of 2–3 mM.

NMR spectroscopy

NMR spectra of duplexes in D_2O and H_2O/D_2O 9:1 v/v were recorded at selected values of $NaClO_4$ concentration (ranging from 0.5 to 6 M) and temperature (303 and 290 K, respectively) using the phase-sensitive method on a Varian Unity$^+$ 500 MHz spectrometer. Proton chemical shifts were referenced to an internal standard of the 3-(trimethylsilyl)-propane sulfonic acid sodium salt (TSPSA) (0.015 p.p.m.). Two-dimensional (2D)-NOESY spectra in D_2O were collected using standard pulse sequence at three different mixing times τ_m= 80, 150 and 250 ms at 303 K. Spectra were acquired with 2K complex data points in the t_2 and 720 real points in the t_1 dimension, with spectral width set to 4.4 kHz in both dimensions. A relaxation delay of 2.5 s between transients was used. 2D-NOESY spectra in H_2O/D_2O 9:1 v/v were acquired at 290 K, mixing time 300 ms, 4K complex points in t_2 and 580 real points in t_1 with spectral width set to 10 kHz in t_2 and 5.5 kHz in t_1 dimension. The WATERGATE method (28) was used to suppress the water signal. DQF-COSY spectra were measured at 303 K with and without ^{31}P decoupling. Spectra were collected with 1K t_1 FIDs of 4K complex points in t_2. Spectral widths were set to 4.3 and 2.1 kHz in t_2 and t_1 dimensions, respectively. ^{31}P NMR spectra were collected with and without proton decoupling at different salt concentration and temperature at 121.4 MHz. 2D heteronuclear ^{31}P–^{1}H chemical shift correlation HETCOR spectra (29) were recorded in 6 M $NaClO_4$. Phosphorus chemical shifts were measured using triethylphosphate as an internal standard and referenced to H_3PO_4. At 6 M $NaClO_4$, the standard has a chemical shift of −0.78 p.p.m., as referenced to external H_3PO_4. The chemical shifts values (Table S1) and other data denoted with the letter 'S' are placed as Supplementary Material available at NAR Online.

Resonance assignments and collection of conformational restraints

Complete resonance assignment of non-exchangeable protons of $(CGCGCG)_2$ was based on 2D-NOESY and DQF-COSY spectra recorded in 6 M $NaClO_4$ in D_2O and analysed with VNMR (Varian) and FELIX (Accelrys) software. Spectra of the $(CGCGCG)_2$ in 6 M $NaClO_4$, show the presence of ∼90% of left-handed form at 303 K. The resonance assignment was based on the new NOE connectivity path [H6$_{(n)}$-H5′/H5″$_{(n)}$-H8$_{(n+1)}$-H1′$_{(n+1)}$-H6$_{(n+2)}$] described here for left-handed helices (see Results and discussion). Imino and amino proton resonances of guanosines and cytidines, respectively, were identified using 2D-NOESY spectra in H_2O/D_2O 9:1 v/v solution. ^{31}P resonance assignments were based on ^{31}P–^{1}H chemical shift correlation experiments (29).

NOE intensities were determined by integration of cross peaks in 2D-NOESY spectra optimized with Lorentzian line shape function. Distance restraints were derived from NOESY spectra at mixing times of 80, 150 and 250 ms using the r^{-6} distance relationship. Calibration was done assuming a distance of 2.45 Å between cytidine H5 and H6 protons. For all NOE distances, distance restraints error bounds were given as follows: 10% lower error bounds and 20% upper error bounds. All $J_{1',2'}$ coupling constants were estimated from the analysis of line shapes in one-dimensional (1D) ^{1}H-NMR spectra. The coupling constants $J_{2',3'}$ and $J_{3',4'}$ were calculated from sums of couplings delivered from ^{31}P decoupled DQF-COSY spectra. The $J_{1',2'}$, $J_{2',3'}$ and $J_{3',4'}$ couplings were interpreted using the generalized Karplus equation in terms of ribose ring pseudo-rotation phase angles (P) and puckering amplitudes (Φ) (30), all calculated with the program PSEUROT v. 6.2. Based on the results obtained, torsion angle restraints for ν_1, ν_2 and δ of each nucleotide residue were determined (coupling constants—see

Table S2). Torsion angle restraints for γ were estimated from low intensity H4′–H5′ and H4′–H5″ contours in the DQF-COSY spectra. Heteronuclear $^3J_{P,H}$ couplings determined from deconvolution of 1D ^{31}P spectra, cross-peaks analysis of both coupled and decoupled DQF-COSY spectra and from the peak intensity analysis of the ^{31}P–^1H HETCOR spectra were employed for the estimation of β and ε torsion angle restraints. Restraints for the *N*-glicosidic bond torsion angle χ were delivered from intra-residual NOE between H8/H6 and H1′ protons in relation to the reference NOE between H5–H6. Lower and upper limits for torsion angle restraints were improved using REDAC cycles (31).

Structure determination

The determination of the (CGCGCG)₂ high salt structure was based on the torsion-angle dynamics algorithm (TAD) (32) implemented in the CYANA v.1.0 program (Güntert,P.). Throughout the work, standard parameters of simulated annealing (*anneal.cya*) were applied with the use of spectroscopic restraints whose number varied depending on the calculation stage (Table 1). The applied protocol (Figure S2) starts from an automatic 2D-NOESY cross-peak assignment based on a subroutine (*assign*) (33) in CYANA for which template duplexes have to be generated. Therefore, 50 random

oligonucleotide chain conformers containing two CGCGCG sequences 5′→3′ joined via a generic linker (using *cyana.lib*) were subjected to the TAD-simulated annealing protocol with a small number of initial restraints (Table 1, Table S4). Twenty duplex structures generated with the lowest target function values were selected as templates and subjected to an automatic 2D-NOESY assignment. To perform the latter, a complete list of ^1H chemical shifts (Table S1) and 1128 unassigned diagonal and cross peaks of the 2D-NOESY spectrum (positions, volumes) at 250 ms, were used. From 548 assigned NOE cross peaks, 165 were with a unique assignment and 419 with multiple assignments (among the latter, 360 were with values over 0.8 in terms of the CYANA's NOE assignment probability). After an analysis of the cross-peaks multiplicity and filtering, 298 assigned NOE cross peaks were obtained for calibration in order to provide initial sets of lower and upper distance restraints for subsequent use as an input to the structure calculation (Figure S2).

At the stage of structure calculation (Figure S2), the TAD algorithm was implemented to the *ndrs.cya* subroutine described here (see Supplementary Material) and operating in CYANA, which allows for an automatic NOE *d*istance *r*estraints *s*election. This module works in cycles and removes the most violated NOE distance restraints. In the first cycle, 50 random oligonucleotide chain conformers (same as above) were subjected to the TAD algorithm with the use of all experimentally derived NOE distance and torsion angle restraints, restraints to enforce the standard Watson–Crick base pairing geometry, and restraints for sugar bond closure (for statistics see Table 1). The resulting 20 duplex structures with the lowest target function values were then analysed for NOE restraints violation. In the first *ndrs.cya* selection cycle, upper and lower NOE distance restraints violated in all 20 structures were discarded. The remaining set of restraints was applied to a next calculation cycle. In four cycles, NOE distance restraints that were violated at least 15, 10, 5 and 2 times among the 20 duplexes, respectively, were removed. Subsequently, torsion angle restraints were qualified using five cycles of the REDAC program (31) (Figure S2) which narrows the range of torsion angle restraints and adds restraints, e.g. for α and ζ angles which are not directly assessed by the experiment. Out of 50 duplex structures, 20 produced by the last REDAC cycle, with the lowest target function values, were accepted (average non-hydrogen atom pairwise r.m.s.d. of 0.72 ± 0.19 Å), and their coordinates together with experimental restraints converted to the X-PLOR format.

Table 1. Statistics for the structure determination and refinement of (CGCGCG)₂ in the Z-RNA form

Structure determination (CYANA)		
NMR restraints		
Initial dihedral angles by J-couplings	64	
Initial dihedral χ angles from NOE	12	
Watson–Crick pair distances	18	
Planarity of base pairs	6	
Ring closure distances	60	
NOE lower and upper distance limits	Before[a]	After[b]
	ndrs.cya	*ndrs.cya*
Upper intra-residue	136	128
Upper inter-residue	162	120
Lower intra-residue	136	120
Lower inter-residue	162	144
Final dihedral angles by REDAC	110	
Analysis of 20 structures with the lowest target function values		
Residual target function	0.59 ± 0.13 Å²	
Number of NOE violations (>0.2 Å)	Upper (0)	lower (0)
Number of torsion angle violations (>5°)	0	
Avg. non-hydrogen atom pairwise r.m.s.d. (0.72 ± 0.19 Å)		
Structure refinement (X-PLOR)		
NMR restraints		
Watson–Crick pair distances	18	
Planarity of base pairs	6	
NOE intra-residue distances	120	
NOE inter-residue distances	112	
Dihedral angles	100	
Total restraints/residue	30	
Analysis of the best 12 conformers		
Average deviation from ideal geometry		
Bond length	0.00253 ± 0.00003 Å	
Bond angles	0.688 ± 0.002°	
Number of NOE violations (>0.2 Å)	0	
Number of torsion angle violations (>5°)	0	
Avg. non-hydrogen atom pairwise r.m.s.d.	0.26 ± 0.12 Å	
NMR *R* factor	0.068 ± 0.001	

[a]Before the first cycle: r.m.s.d, 1.50 Å; avg. target function value, 42.83 Å² (for the family of the best 20 structures).
[b]After the fifth cycle: r.m.s.d, 0.68 Å; avg. target function value, 0.77 Å² (for the family of the best 20 structures).

Structure refinement and analysis

The 20 accepted CYANA conformers representing the Z-form of (CGCGCG)₂ were refined using the X-PLOR v. 3.851 program (Brünger,A.T.) with the Charmm force field (*DNA–RNA-allatom.param*) and topology (*DNA–RNA-alla-tom.top*) parameters (34) applying the gentle refinement protocol in Cartesian space (35). The protocol includes an initial conjugate gradient minimization (number of steps 600) subsequent simulated annealing (200 K, number of steps 10 000, time step 0.0005 ps) and a final conjugate gradient minimization (number of steps 1000). In all three stages, experimental restraints and restraints for the base planarity (optimized force constant value 20 kcal mol⁻¹ Å⁻¹)

were used (Table 1). The refinement resulted in an ensemble of 12 accepted conformers with proper stereochemistry and restrained distances and dihedral angles that deviated from their set ranges by <0.2 Å and 5°, respectively. These structures are characterized by a low average, non-hydrogen atom, pairwise r.m.s.d. of 0.26 ± 0.12Å. To assess the quality of the final structure set, the NMR *R* factor was used as a measure for the fit of the refined coordinates to the NOESY data. Its value of 0.068 ± 0.001 corresponds to $\tau_m = 250$ ms and to calculated optimal rotational correlation time of 2 ns. Helical parameters (36) for the set of 12 final structures were evaluated using the program CURVES v. 5.11. All conformational parameters were subjected to statistical analysis. The coordinates of the Z-form (CGCGCG)$_2$-refined structure set and the list of molecular restraints have been deposited (37) in the Protein Data Bank (PDB).

The model of the full-turn left-handed RNA helix was generated as follows. From all 12 refined structures of (CGCGCG)$_2$, the 5′ and 3′ terminal base pairs were cut off and coordinates of the resultant set of the (pGCGC)$_2$ core duplexes were averaged. The (pGCGC)$_2$ core was treated as a building block for the helix extension. This was done by overlapping the upstream half base pairs [pG(4)C(5)]$_2$ with the downstream half [pG(2)C(3)]$_2$ of the next (pGCGC)$_2$ building block. Because conformational properties of [G(2)C(3)]$_2$ and [G(4)C(5)]$_2$ are different (Figure 2, Table 2), though to a very small extent, coordinates of the overlapping GC base pairs were averaged. Elongation steps were repeated five times to obtain a 14mer double-stranded (GC)$_7$ construct. Terminal base pairs were then removed and the 12mer construct (CG)$_6$ was subjected to a short energy minimization in order to fix the internucleotide phosphodiester linkages. The rest of the helix structure was kept restricted using experimental restraints in order to avoid force-field-induced conformational changes of the model.

RESULTS AND DISCUSSION

### Resonances assignment—the NOE connectivity path for left-handed double helices

As shown earlier for the low salt spectra of right-handed RNA helices (4), the length of the (CGCGCG)$_2$ is the minimum which would reveal different properties of CpG and GpC steps. The much pronounced effect of alternation in the structure and the line broadening at high salt concentration, make it difficult to perform an accurate NMR analysis of a mixture of A- and Z-forms of (CG)$_n$ duplexes, even of that length. For A-RNA and B-DNA helices, the routine procedure of resonance assignment within the aromatic/anomeric region of the NOESY spectra is based on the existence of the [H8/H6$_{(n)}$-H1′$_{(n)}$-H8/H6$_{(n+1)}$] NOE connectivity path (38). In the spectra of left-handed helices of both DNA (10,11,39,40) and RNA (17), this sequence-specific connectivity is broken because the (deoxy)guanosine residue in a *syn* conformation is positioned at a distance too far from the 5′ neighbouring (deoxy)cytidine to detect NOE. Therefore, in early studies of (CGCGCG)$_2$ (17), another method of assigning resonances in the left-handed form was used, taking advantage of the slow kinetics of the *A to Z* transition (the ratio 1:1 was observed for both forms in 4 M NaClO$_4$ at 297 K). In a system exchanging

so slowly, cross peaks resulting from chemical exchange appeared in parallel to those produced by NOE, which makes it possible to correlate the assigned proton resonances in the aromatic/anomeric region of the right-handed form with the same protons in the left-handed form (39,40).

Having measured the salt- and temperature-dependence of the A- to Z-form ratio we decided to analyse the spectra of (CGCGCG)$_2$ in 6 M NaClO$_4$, which show the presence of ~90% of left-handed form at 303 K (Figure S1). These conditions were also chosen in order to get a closer correlation with data reported previously (17). The 2D-NOESY spectrum shows very strong cross peaks resulting from intranucleotide H1′–H8 NOEs indicating the *syn* conformation of all three guanosine residues. The analysis of the NOESY spectra at mixing times $\tau_m = 150$ and 250 ms indicated that an assignment based on the 'walk along helix' is also possible for Z-helices, due to the existence of the NOE connectivity path: H6$_{(n)}$-H5′/H5″$_{(n)}$-H8$_{(n+1)}$-H1′$_{(n+1)}$-H6$_{(n+2)}$ (Figure 1). This wide-ranging path allows a straightforward cross-peak assignment of most non-exchangeable resonances for the Z-RNA form (Table S1). The application of this pathway eliminates the necessity of an analysis of near-diagonal regions in spectra containing both A- and Z-forms and allows for an unambiguous assignment of salt concentration-dependent chemical shifts for the Z-RNA form. Moreover, due to the considerable upfield shift of cytidine H5″ and especially H5′ proton resonances (2.5–3.0 p.p.m.), the H5′/H5″-H1′$_{(n+1)}$ cross peaks to 3′ neighbouring guanosines were observed. This, together with intranucleotide cross peaks, allowed a complete assignment in the aromatic/anomeric region.

Other non-exchangeable proton resonances were fully assigned from the analysis of other regions of DQF-COSY and 2D-NOESY spectra. For cytidine residues, H1′ resonances were identified based on intranucleotide NOEs to H6. The assignment of others ribose resonances were obtained from H1′–H2′, H2′–H3′, H4′–H5′, H4′–H5″ correlation signals in the DQF-COSY spectra. Strong H1′–H2′ correlation and no correlation signals for H3′–H4′ indicate an S-type puckering for all cytidines. Stereospecific assignment for H5′/H5″ was possible due to the presence of resolved H3′–H5′/H5″ internucleotide cross peaks in 2D-NOESY spectra ($\tau_m = 80$, 150 ms). In case of G2 and G4 residues, H1′ resonances appear as singlets over a wide range of temperature, while H1′ of G6 shows up as a doublet with weak coupling with H2′. The latter indicates a considerable fraction of S-type puckering (32%) for G6. H2′ resonances of G2 and G4 were assigned from intranucleotide H8–H2′ NOEs. All H3′ and H4′ signals of guanosine residues were assigned based on H2′–H3′ and H3′–H4′ correlations in the DQF-COSY spectra. Both strong H3′–H4′ correlation and no H1′–H2′ coupling indicate the N-type conformation for G2 and G4 residues. Guanosine H5′/H5″ proton signals were identified from the analysis of H3′-H5′/H5″ internucleotide cross peaks in 2D-NOESY spectra. Guanosine H5′/H5″ signals resonate very close to each other, to H4′ and to a water signal, which makes their stereospecific assignment difficult.

Assignments of exchangeable protons. Due to exchange processes under high salt conditions, the signals of amino protons for guanine residues are not observable. Imino proton signals of G2 and G4 are sharp and well separated; the signal of G6 is
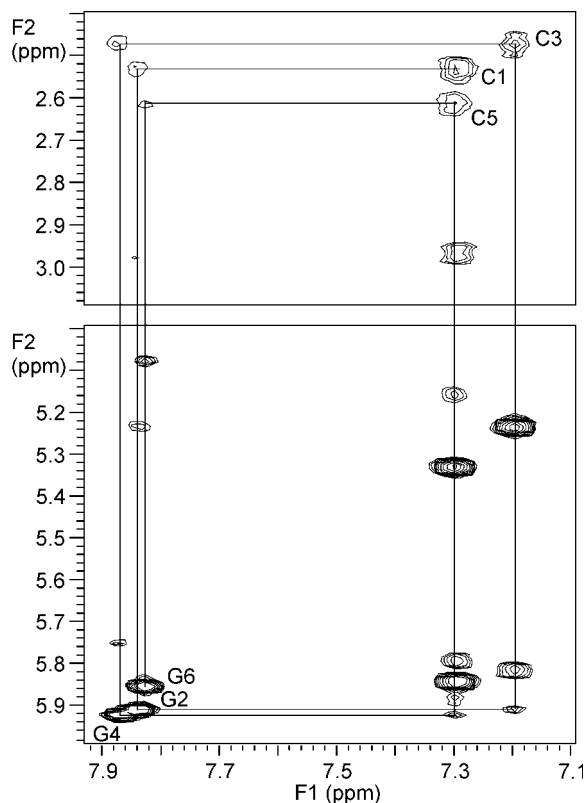
Figure 1. Contour plot of the 2D-NOESY spectrum (250 ms) of (CGCGCG)$_2$ in the Z-RNA form showing wide-ranging connectivity path [H6$_{(n)}$-H5′/H5″$_{(n)}$-H8$_{(n+1)}$-H1′$_{(n+1)}$-H6$_{(n+2)}$] for Z-helices. Intra-residue cross peaks of cytidine H6–H5′ and guanosine H8-H1′ are marked.

broad. The amino proton resonances for C1, C3 and C5 are much broader. For the chemical shift values see Table S1. The assignment of imino protons for all guanosines was accomplished from the NOESY spectra in H$_2$O/D$_2$O 9:1 v/v using cross peaks of NH (G) with NH$_2$ (C), being characteristic of Watson–Crick base pairing. This interaction was preserved up to 6 M NaClO$_4$ and at the temperature range of 273–323 K. Imino and cytidine amino protons of all but terminal residues were observed to form intra- and inter-strand cross peaks with non-exchangable protons.

Assignments of phosphorus nuclei. ^{31}P NMR spectrum of (CGCGCG)$_2$ in 6 M NaClO$_4$ is characteristic of two dispersed signal groups which, as indicated (17), are related to CpG and to GpC steps, respectively. Individual ^{31}P resonances for the Z-RNA duplex have not been assigned so far. Here, three well separated signals observed for CpG steps at −1.01, −1.20 and −1.24 p.p.m. were assigned to G2, G6 and G4 residues, respectively, from strong P-H3′ correlation in the ^{31}P–^{1}H HETCOR spectra. For GpC steps, both C3 and C5 phosphorus signals resonate at 0.04 p.p.m. As seen from the HETCOR spectra, C5 is less shielded than the C3 phosphorus resonance and both are coupled through three bonds to H3′ and H5′/H5″. Much weaker coupling is observed for the four-bond coupling to H4′ (P-O5′-C5′-C4′-H4′). Coupling constants ^{3}J$_{P,H3′}$ (6–7 Hz), of all nucleotide residues, and ^{3}J$_{P,H5′}$ and ^{3}J$_{P,H5″}$ (3–4 Hz) for C3 and C5 were obtained from the analysis of both coupled and decoupled DQF-COSY spectra. ^{3}J$_{P,H5′}$ and

^{3}J$_{P,H5″}$ couplings are <3 Hz, as inferred from their absence in the HETCOR spectra. All the ^{31}P–^{1}H coupling constants were employed for an estimation of initial restraints for β and ε torsion angles (Table S3).

Structure determination and refinement

The (CGCGCG)$_2$ structure was determined using the torsion-angle dynamics algorithm (TAD) (32) and the CYANA software. Line broadening in Z-RNA spectra at high salt makes it difficult to access the large amount of conformational restraints. To enlarge the number of high quality restraints at the structure calculation stage, the new subroutine for the automatic *N*OE *d*istance *r*estraints *s*election (*ndrs.cya*) was introduced to CYANA (Figure S2). From 596 initial NOE restraints, 84 inconsistent restraints (14%) were removed (Table 1). Those rejected were related either to erroneous NOE volume measurement due to the base line drift and cross-peaks overlapping (including those from the residual A-form) or, potentially, to spin diffusion. The *ndrs.cya* subroutine (Supplementary Material) when coupled with REDAC cycles delivering qualified torsional angle restraints (31) has provided us with the access to 30 restraints per nucleotide residue (Table 1). The calculated left-handed duplex, represented by a set of 20 accepted structures with the lowest target function values, was already well defined (average non-hydrogen atom pairwise r.m.s.d. 0.72 ± 0.19Å). Since the CYANA program does not optimize against a general energy force field that would also account for electrostatic interactions, the group of all 20 accepted duplex structures was refined using a gentle refinement protocol (36) of the X-PLOR program (for statistics see Table 1). This was done with caution and not without hesitation since the available force fields are not well suited to treat molecule electrostatics for such a very high salt concentration that was used for structure determination. It should be emphasized that during the gentle refinement, the full set of experimental restraints was applied. The influence of the force constants for the base planarity restraints on the structure was analysed by monitoring both the structure r.m.s.d. and its respective helical parameter values. Within the range of 0–50 kcal mol^{-1} Å^{-2}, the force constant value 20 kcal mol^{-1} Å^{-2} was found optimal (for the force constant equal to zero, the propeller twist angles of terminal base pairs rise to the unaccepted value of 20°; parameters describing internal base pairs were changed by a small extent only). The refined structure of the left-handed (CGCGCG)$_2$ generated is finally represented by a set of 12 conformers (r.m.s.d. 0.26 ± 0.12Å) (37).

Structural features of the left-handed double helix (Z-RNA)

The refined structure of (CGCGCG)$_2$ determined in 6 M NaClO$_4$ is a half turn of a left-handed RNA helix (Figure 2). Currently, coordinates of about 60 X-ray structures of Z-DNA of different sequence and only two NMR structures of an 8-methylguanosine containing d(CG)$_3$, both determined at low salt (10,11), have been deposited in PDB. Here, when comparing conformational features of the Z-form (CGCGCG)$_2$ to Z-DNA, we will refer (Table 2, Table S3) only to the 11 X-ray structures of unmodified Z-form
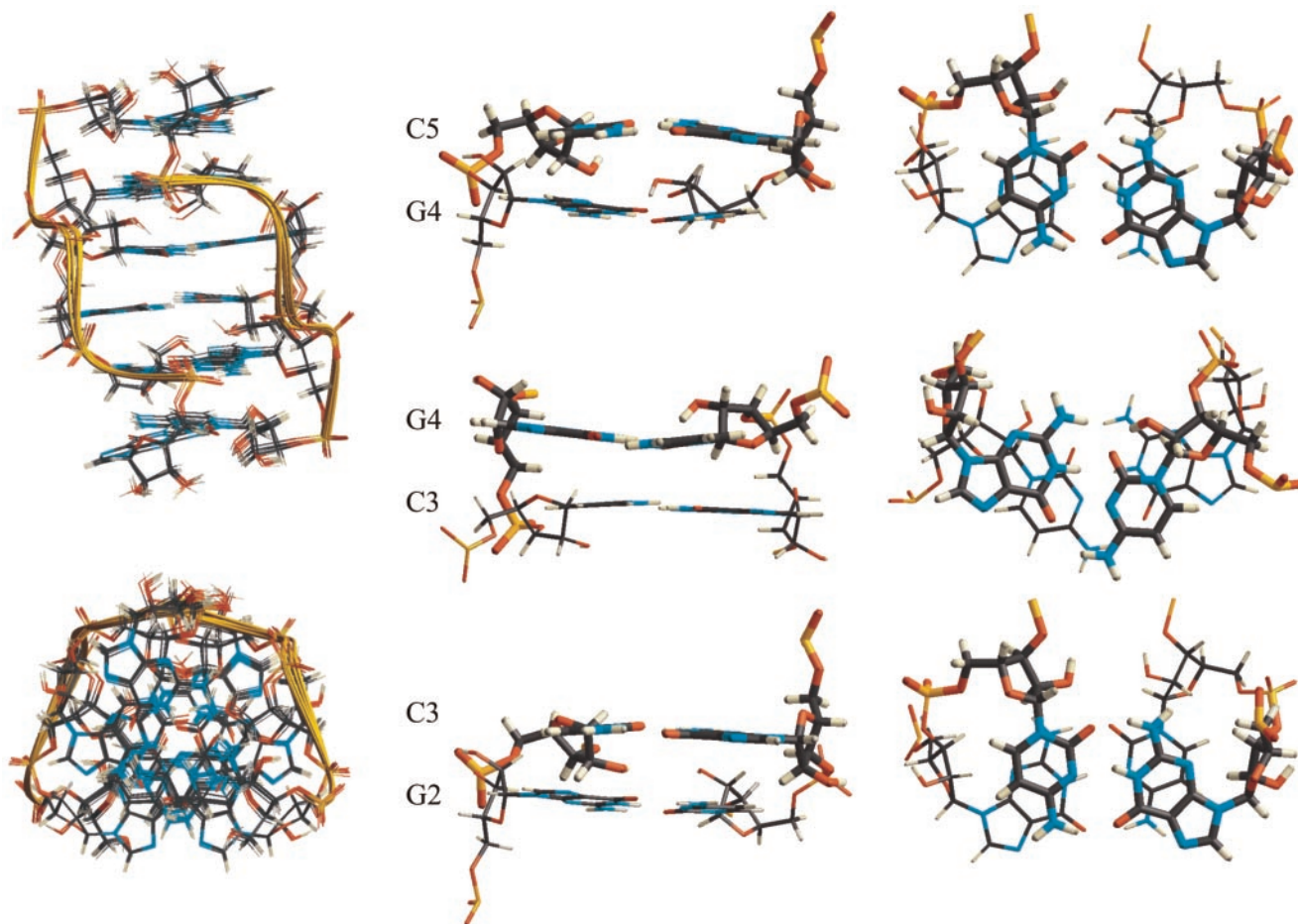
Figure 2. First column: superposition of 12 conformers representing the refined structure of (CGCGCG)$_2$ in the Z-RNA form as viewed from the minor groove and along the helix *z*-axis. Second and third column: stacking pattern within the CpG and GpC steps in Z-RNA as viewed from the minor groove and along the helix *z*-axis. For both steps only intra- but no inter-strand stacking is observed.

d(CGCGCG)$_2$, for which coordinates are available. The low salt NMR structure of d[CGC(m^{8}G)CG]$_2$ (10), (PDB ID: ITNE), differs in several points from both Z-DNA crystal structures and Z-RNA (data not shown). Because of the 8-methyl-substitution of the guanine ring we will not refer to that structure in detail.

Ribose, glycosidic bond and backbone conformation. J$_{1',2'}$, J$_{2',3'}$ couplings of both cytidine and guanosine residues, derived from DQF-COSY spectra, were the same (within ±0.2 Hz) as reported earlier for (CGCGCG)$_2$ at identical salt and temperature conditions (17). However, our J$_{3',4'}$ for G2 and G4 residues were ~1 Hz larger (Table S2). This makes pseudorotation phase angle values for G2 and G4 also higher (PSEUROT: P_N range 30–40°, average $\Phi = 38°$), indicating a C3'-*endo*/C4'-*exo* conformation. In all 12 refined Z-RNA structures, guanosines show the C4'-*exo* pucker (Table S2). The same pucker of the G residue was reported for a ribo-CpG step within the crystal structure of chimeric [d(CG)r(CG)d(CG)]$_2$ (15). A conformational lability of the G6 terminal sugar residue was observed (J$_{1',2'}$ = 3.8 Hz), although with preference for the N-pucker. All guanosine residues are characterized by a syn conformation with χ

angle values (nearly 61) similar to those observed in Z-DNA. All cytidine residues adopt an unusual for RNA, C2'-*endo* sugar puckering. However, data given by PSEUROT and those obtained by the model analysis indicate a range of pseudorotation phase angle values much wider than typical (P_S range 135–200°, average $\Phi = 38°$). All cytidine residues adopt the anti conformation of *N*-glycosidic bonds (Table S3).

Table S3 shows the α, β, γ, δ, ε, ζ backbone torsion angles derived from the final 12 refined Z-form (CGCGCG)$_2$ structures. It should be emphasized that d(CpG) internucleotide linkages in all X-ray Z-DNA hexamer structures are nearly identical while for d(GpC) two different conformations denoted Z$_I$ and Z$_{II}$ are characteristic (41,42). In the Z$_{II}$ conformation, the phosphate group is rotated and hence shifted, relative to Z$_I$, towards the 3' end of the hexamers (41). Therefore, both Z$_I$ and Z$_{II}$ differ in values of ε and ζ angles for deoxyguanosine residues and in α, β angles for deoxycytidines. The direct estimation of α and ζ angles from ^{3}J couplings is impossible. Moreover, determination of α and ζ angles from ^{31}P chemical shifts analysis would be erroneous due to a considerable effect of salt concentration. A description of restraints for both those angles was possible due to an

Table 2. Selected helical parameters[a] for 12 conformers representing the refined structure of (CGCGCG)$_2$ in the Z-RNA form (left column) and 11 reference X-ray Z-DNA structures[b] of d(CGCGCG)$_2$ (right column)

Base pairs	x-Displacement [Å]		y-Displacement [Å]		Inclination [°]		Propeller twist [°]	
C1-G12	0.1 (0.1)	−2.5 (0.2)	−1.5 (0.2)	−2.1 (0.2)	10.7 (0.7)	7.1 (1.1)	13.2 (1.2)	−0.1 (1.0)
G2-C11	−0.2 (0.1)	−2.4 (0.2)	1.5 (0.2)	2.3 (0.2)	8.7 (0.7)	7.7 (1.3)	−1.0 (1.5)	−1.4 (2.9)
C3-G10	−0.2 (0.1)	−2.4 (0.2)	−1.4 (0.2)	−2.2 (0.2)	7.4 (0.8)	7.5 (1.2)	−1.9 (0.7)	−0.3 (4.8)
G4-C9	−0.1 (0.1)	−2.4 (0.2)	1.5 (0.2)	2.3 (0.2)	7.3 (0.9)	7.1 (1.2)	−1.9 (0.6)	1.2 (2.5)
C5-G8	−0.3 (0.1)	−2.5 (0.3)	−1.4 (0.2)	−2.2 (0.1)	8.5 (0.9)	6.4 (1.3)	−1.4 (2.0)	−1.7 (2.9)
G6-C7	0.2 (0.1)	−2.3 (0.2)	1.6 (0.2)	2.3 (0.2)	10.4 (0.8)	6.9 (1.1)	13.2 (0.7)	3.7 (1.7)

Base steps	Twist [°]		Rise [Å]		Slide [Å]		Tilt [°]	
C1/G2	7.2 (0.7)	−8.9 (1.5)	3.6 (0.1)	4.3 (0.1)	3.1 (0.1)	4.4 (0.1)	−4.0 (1.0)	0.7 (1.2)
G2/C3	−60.8 (1.7)	−51.3 (1.3)	3.5 (0.2)	3.1 (0.1)	−2.9 (0.1)	−4.4 (0.1)	−3.5 (1.2)	−0.4 (0.4)
C3/G4	4.1 (0.9)	−8.4 (0.7)	3.0 (0.1)	4.4 (0.1)	2.8 (0.1)	4.5 (0.1)	−0.1 (0.6)	−0.9 (1.0)
G4/C5	−61.3 (1.5)	−50.8 (0.9)	3.6 (0.2)	3.0 (0.1)	−2.9 (0.1)	−4.5 (0.2)	3.3 (1.7)	−0.6 (1.6)
C5/G6	7.4 (0.9)	−9.8 (0.9)	3.6 (0.1)	4.1 (0.1)	3.1 (0.1)	4.4 (0.2)	3.7 (0.8)	0.9 (0.6)

[a]Average values with standard deviations are given in parentheses; calculated with CURVES (36).
[b]PDB ID: 131D, 1D39, 1D48, 1DCG, 1DJ6, 1I0T, 1ICK, 292D, 293D, 2DCG, 336D.

introduction of a large number of NOE restraints to the structure determination protocol applying REDAC cycles. This allows us to show that the conformations of GpC linkages in Z-RNA structure at high salt are close to those of the Z$_I$ type.

Base pairs and stacking geometry. Table 2 shows a comparison of helical parameters for a set of 12 conformers (r.m.s.d. 0.26 ± 0.12Å) of the Z-RNA duplex and for X-ray Z-DNA reference structures. The Watson–Crick scheme of base pairing is observed throughout the duplex. The propeller twist angles for base pairs, excluding the terminal ones, are small. Also other global base–base parameters are of small value, as in Z-DNA. Due to small *x*- and *y*-displacement values, base pairs in Z-RNA are much closer to the *z*-axis, i.e. ~1.7 and 0.9 Å than in the case of X-ray Z-DNA structures and NMR structure of d[CGC(m^{8}G)CG]$_2$ (10), respectively. The inclination angles are a little higher (~9°) than in the case of Z-DNA. Contrary to the Z-DNA, there is no alternation of the rise parameter for both CpG and GpC steps. In the core of the Z-RNA duplex, the helical rise is 3.2 Å and its value at the CpG step is lower than in the Z-DNA by >1 Å.

In contrast to Z-DNA X-ray structures for which the helical twist angle between successive base pairs varies between low negative values for CpG steps (−10 to −8°) and much lower value for GpC steps (−53 to −49°), in the Z-RNA duplex this angle is low and positive (4–7°) at CpG steps and highly negative (−61°) for GpC steps. This latter feature has a strong effect on the Z-RNA stacking pattern. For the GpC step, base stacking interactions are strongly intra-strand, as seen in the Z-DNA. However, for CpG steps we also observed intra-strand but evidently no inter-strand base stacking (Figure 2), which is a common feature of Z-DNA structures. Some additional stabilization is gained due to 'on the edge' stacking of the imidazole ring of guanine with the O4′ oxygen of the adjacent cytidine. Such a striking stacking geometry allows return to the previously raised question (8,17,44) whether Z-RNA belongs to a new family of left-handed helices. In view of the early reports (43,44) on considerable differences between Z-DNA and Z-RNA oligonucleotide duplexes observed by CD and Raman spectroscopy—methods very sensitive to stacking—we now have evidence to support an affirmative answer to that question.

Global structure of the Z-RNA helix. To generate the model of a full-turn Z-RNA helix, both terminal base pairs of the left-handed (CGCGCG)$_2$ structure were excluded from parameterization (see Materials and Methods). Conformational features of (CGCGCG)$_2$ described above have a pronounced effect on the global structure of the full-turn model of the Z-RNA helix (Figure 3). The left-handed RNA helix contains 12.4 bp per turn and has a well-marked, known from the Z$_I$-DNA model, *zig-zag* shape of the phosphorsugar backbone. However, the Z-RNA model is significantly different from the Z$_I$- and especially Z$_{II}$-DNA model, both containing 12 bp per turn (41). In Z-DNA helices, CG base pairs are set away from the *z*-axis with their imidazole parts of guanine rings protruding onto the outer helix surface. Base pairs in the Z-RNA helix, due to their smaller *x*- and *y*-displacement parameters, are located much closer to the helix *z*-axis. This spectacular difference is seen when viewing left-handed helices along their *z*-axes (Figure 3). The central hole of Z-RNA is smaller than that of Z$_I$-DNA. Another striking feature is that internucleotide phosphate ions and guanosine 2′-OH groups are strongly exposed to the outer helix surface. This might be considered as a result of the fact that the Z-RNA duplex structure was determined at high salt. In Z-DNA only one groove is observed, corresponding to the minor groove of B-DNA; the major groove seen in B-DNA is restructured in Z-DNA to form a curved surface. On the contrary, in the Z-RNA helix, both grooves are well defined (Figure 3). The minor groove is very well engraved, deep and much narrower than that of the Z-DNA. In the minor groove, cytidine 2′-OH groups are buried. The major groove of Z-RNA is shallow exposing cytidine *exo*-amino groups and guanosine O(6) and C(8)-H sites.

The key role of the cytidine 2′-OH group in Z-RNA structure. The effect of a single 2′-OH group substitution on the Z-DNA duplex structure was studied by X-ray crystallography using chimeric [d(CG)r(CG)d(CG)]$_2$ (15). For that structure, an intra-strand hydrogen bond of the cytidine 2′-OH group with the NH$_2$ function of the 5′-neighbouring deoxyguanosine residue stabilizing its *syn* conformation was postulated. In the Z-form of (CGCGCG)$_2$, a formation of the intra-strand hydrogen bond between the cytidine 2′-OH and the 5′-neighbouring guanosine NH$_2$ group is likely (depending on the step, O–N distance 3.0–3.3 Å) but no direction of that bond could be
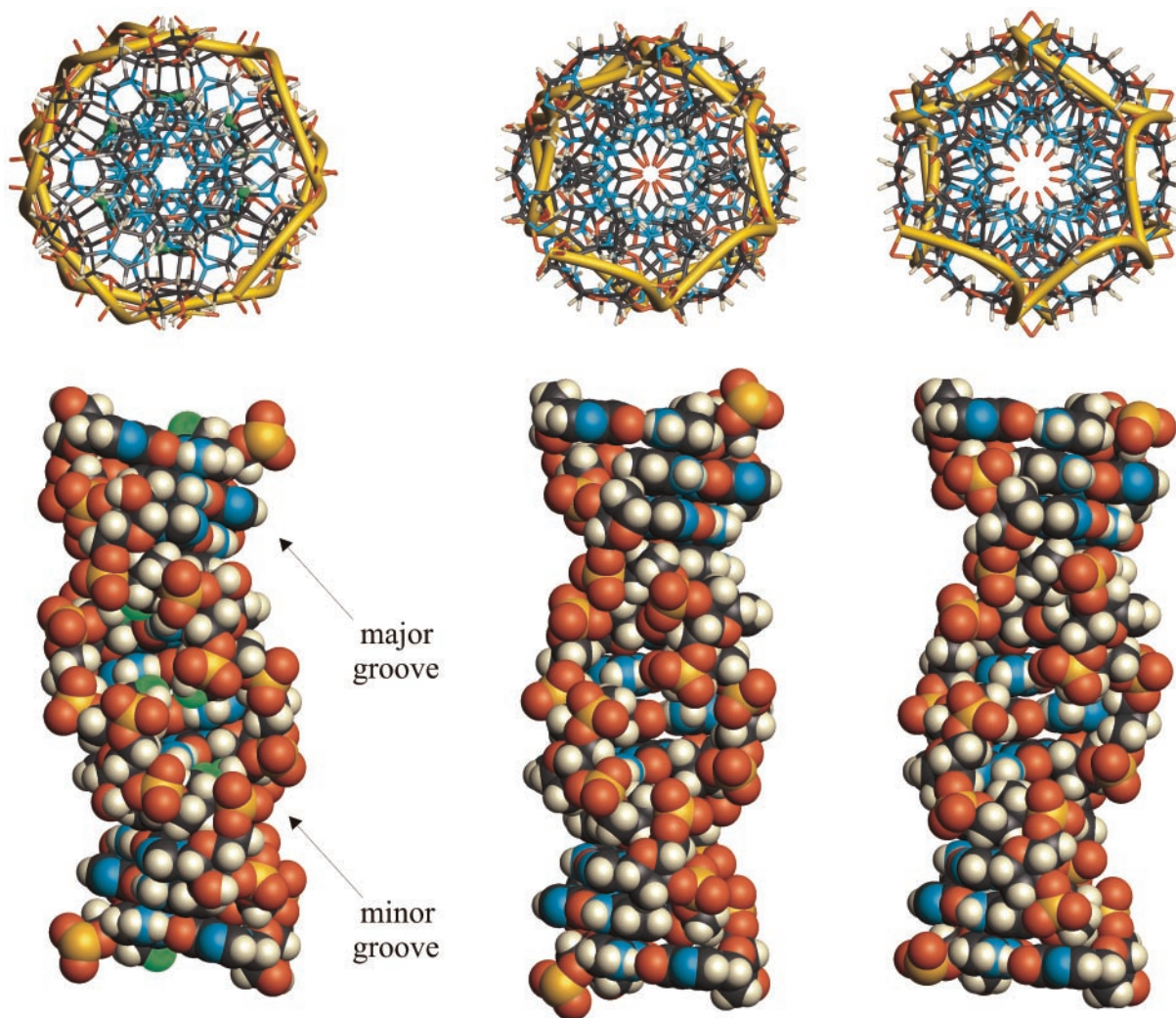
Figure 3. Full-turn model of the Z-RNA helix (12.4 bp per turn) (left) compared to the 12 bp per turn models of Z_I- (middle) and Z_{II}-DNA (right) (41). Models are visualized in two different conventions in order to show their base pair location and groove architecture. Atoms are coloured by type (carbon in black, hydrogen in white, nitrogen in blue, phosphorus in yellow, oxygen in red; cytidine 2′ oxygens are given in green).

postulated (see below). The formation of an alternative hydrogen bond to N3 of the guanine, as found in the crystal structure of a short helix $[C(Br^8G)]_2$ (14), is disfavoured (O–N distance 4.8 Å). An analysis of the CpG and GpC stacking patterns of the $(CGCGCG)_2$ structure (Figure 2) and of the full-turn model of Z-RNA (Figure 3) suggest the structural involvement of cytidine 2′-OH groups in the inter-strand interactions. For GpC cytidines, the O2′ atoms distance between two 2′-OH groups is only 3.1 Å. It remains to be seen whether, in the absence of inter-strand base stacking, such a ribose–ribose close contact would add to the stabilization of the Z-RNA structure. For CpG cytidines, the respective O2′ atoms' distance is 7.8 Å.

The authors of the $[d(CG)r(CG)d(CG)]_2$ X-ray structure proposed a model of the full-turn Z-RNA helix, similar to Z-DNA. That model based only on a partial information concerning the (dG)pC step, shows cytidine 2′-OH groups situated in the minor groove (15). Our full-turn model of the Z-RNA helix based on the high salt structure of $(CGCGCG)_2$ supports this suggestion (Figure 3). 2′-OH groups of cytidine residues are very much buried in the minor groove while 2′-OH of guanosines are directed to the surface of the helix. Although

it remains to be established how water molecules are positioned in the Z-RNA minor groove, we hypothesize on the basis of X-ray crystal structures of 2′-*O*-Me$(CGCGCG)_2$ (5,6) that the cytidine 2′-OH group of the CpG step may also span both RNA strands indirectly via hydrogen bonds to, most probably, a single row of water molecules. Water-mediated ribose–ribose interactions in the minor groove would also add to the stabilization of the Z-RNA structure.

The 2′-OH group of cytidines plays a key role not only in the Z-RNA structure stabilization but also in the process of *A to Z* helicity reversal. This was proved by the residue-specific 2′-*O*-methylation of the $(CGCGCG)_2$ duplex. The 2′-*O*-Me$(CGCGCG)_2$ does not undergo a reversal to Z-RNA even under highly dehydrating conditions induced by 2-methyl-2,4-pentanediol (6) or high pressure (45). These observations were confirmed here using ^{31}P NMR spectroscopy. The 2′-*O*-Me$(CGCGCG)_2$ remains in the right-handed form up to 6 M NaClO$_4$ while the $[C(2′-OMe)G]_3$ undergoes helicity reversal to form both right-handed and Z-forms in a 1:1 ratio in 6 M NaClO$_4$ (Figure 4). In contrast, the $[(2′-OMe)CG]_3$ containing 2′-*O*-methylated cytidine residues does not undergo helicity reversal
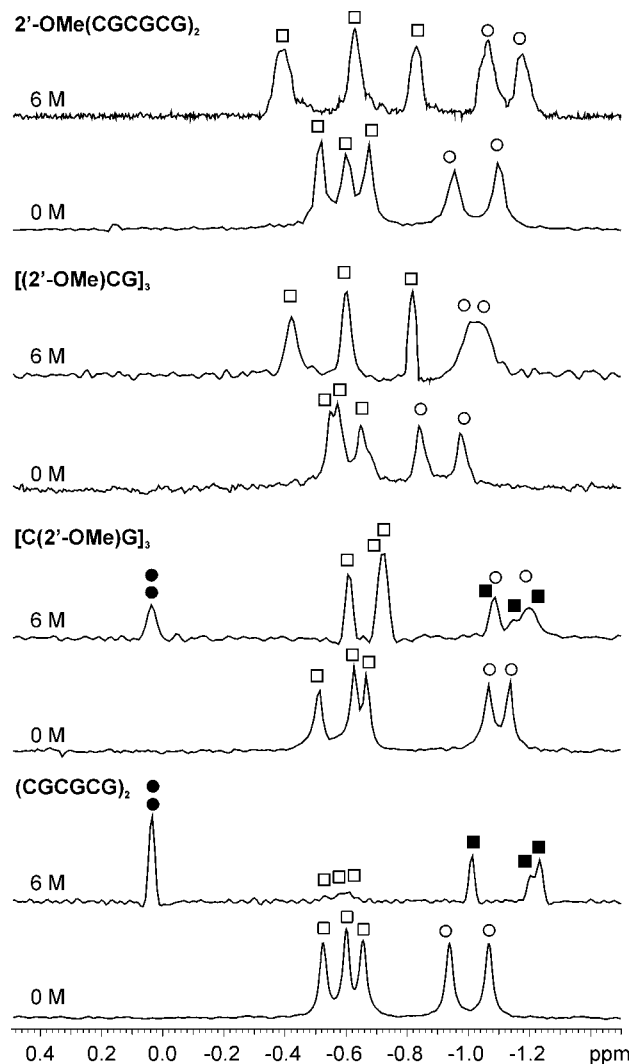
Figure 4. Monitoring of the *A to Z* RNA helicity reversal. From bottom to top: ^{31}P NMR spectra of the (CGCGCG)$_2$, its residue-specific 2′-*O*-methylated analogues [C(2′-*O*Me)G]$_3$, [(2′-*O*Me)CG]$_3$ and of 2′-*O*-Me(CGCGCG)$_2$ at 0 and 6 M NaClO$_4$. ^{31}P chemical shifts of A- and Z-forms are coded as follows: circles, GpC (A); black circles, GpC (Z); rectangles, CpG (A); black rectangles, CpG (Z).

up to 6 M NaClO$_4$. These results are fully in agreement with the structural data presented here. In the Z-RNA, all cytidine residues have to adopt the C2′-*endo* sugar puckering. This conformation is inaccessible to 2′-*O*-methylcytidines which strongly favour C3′-*endo* puckering (4). In any case, the narrow and deep minor groove of the Z-RNA helix would not accommodate the bulk of 2′-*O*-methyl groups. This is in contrast with the case of guanosine residues which would fasten the C3′-*endo* conformation upon 2′-*O*-methylation, also preferred in the Z-form. Moreover, guanosine 2′-hydroxyls are fully accessible in the Z-RNA structure and there is enough space to accommodate the 2′-*O*-methyl groups.

CONCLUSIONS

Within the large family of RNA structural motifs elucidated by NMR and X-ray methods, many of high complexity, we were

missing the left-handed Z-RNA helix. The left-handed RNA prevails at much higher salt concentration than that noted for Z-DNA, making its NMR structure determination challenging. The first solution structure of the left-handed RNA duplex (CGCGCG)$_2$ presented here, is furthermore the first nucleic acid motif determined under salt concentration as high as 6 M NaClO$_4$. When determining the NMR structure of Z-RNA, two methodological novelties were introduced. First, the sequential assignment of non-exchangeable proton resonances of the Z-form was based on a hitherto unreported NOE connectivity path [H6$_{(n)}$-H5′/H5″$_{(n)}$-H8$_{(n+1)}$-H1′$_{(n+1)}$-H6$_{(n+2)}$] for left-handed helices (Figure 1). As kindly suggested by one of the referees, the connectivity [H8$_{(n+1)}$-H2′$_{(n+1)}$-H6$_{(n+2)}$] might serve as an alternative segment of the whole path. The NOE path revealed in our studies should also facilitate NMR studies of Z-DNA and their complexes. The second novelty, an implementation of a subroutine *ndrs.cya* operational in CYANA allows an automatic NOE distance restraints selection at the stage of structure calculation using torsion angle dynamics. Consequently, our determination of the Z-RNA duplex structure was based on a collection of 30 restraints per nucleotide residue. From the conformers delivered by CYANA, 20 with the lowest target function values were subjected to the X-PLOR gentle refinement to obtain the left-handed (CGCGCG)$_2$ structure finally represented by a set of 12 conformers (r.m.s.d. 0.26 ± 0.12 Å). Both the left-handed (CGCGCG)$_2$ structure and the full-turn model of Z-RNA helix generated using its coordinates show several conformational features significantly different from Z-DNA (Table 2, Table S3). Helical twist angles for CpG steps have small positive (4–7°) whereas GpC steps have large negative (−61°) values. The Z-RNA structure shows no inter-strand base stacking (Figure 2). Additional stabilization of the Z-RNA structure is gained due to cytidine 2′-OH groups, which are involved in the inter- and intra-strand interactions. The cytidine 2′-OH group also plays a key role in the RNA helicity reversal as proved by residue specific 2′-*O*-methylation. In the full-turn model of Z-RNA (12.4 bp per turn), base pairs are much closer to the helix axis than in Z-DNA, thus both the very deep, narrow minor groove and the major groove are well defined (Figure 3). A striking feature of Z-RNA structure viewed along *z*-axis is that internucleotide phosphates and guanosine 2′-OH groups are strongly exposed to the outer helix surface, forming a hydrophilic sphere.

We hope that our results will be of general interest to those studying structures of RNA and would be helpful in evaluation of the events in the RNA replication machinery, which involve a conformational strain (19,46). Having determined coordinates of RNA (CG)$_n$ duplexes, both in the right-handed form (4) and in the left-handed form, presented here, we are focusing now on elucidation of the mechanism of *A to Z* helicity reversal. Knowledge about the Z-RNA structure would also be of interest for the studies of left-handed RNA interactions with Zα domain proteins, e.g. RNA-editing enzyme ADAR1.

SUPPLEMENTARY MATERIAL

Supplementary Material is available at NAR Online.

ACKNOWLEDGEMENTS

REFERENCES

1. Wang,A.H.-J., Quigley,G.J., Kolpak,F.J., Crawford,J.L., van Boom,J.H., van der Marel,G. and Rich,A. (1979) Molecular structure of a left-handed double helical DNA fragment at atomic resolution. *Nature*, **282**, 680–686.

2. Hall,K., Cruz,P., Tinoco,I.,Jr, Jovin,T.M. and van de Sande,J.H. (1984) 'Z-RNA'. A left-handed RNA double helix. *Nature*, **311**, 584–586.

3. Adamiak,R.W., Galat,A. and Skalski,B. (1985) Salt- and solvent-dependent conformational transitions of ribo-CGCGCG duplex. *Biochim. Biophys. Acta*, **825**, 345–352.

4. Popenda,M., Biala,E., Milecki,J. and Adamiak,R.W. (1997) Solution structure of RNA duplexes containing alternating CG base pairs: NMR study of r(CGCGCG)$_2$ and 2'-*O*-Me(CGCGCG)$_2$ under low salt conditions. *Nucleic Acids Res.*, **25**, 4589–4598.

5. Adamiak,D.A., Milecki,J., Popenda,M., Adamiak,R.W., Dauter,Z. and Rypniewski,W.R. (1997) Crystal structure of 2'-*O*-Me(CGCGCG)$_2$, an RNA duplex at 1.30 Å resolution. Hydration pattern of 2'-*O*-methylated RNA. *Nucleic Acids Res.*, **25**, 4599–4607.

6. Adamiak,D.A., Rypniewski,W.R., Milecki,J. and Adamiak,R.W. (2001) The 1.19 Å X-ray structure of 2'-*O*-Me(CGCGCG)$_2$ duplex shows dehydrated RNA with 2-methyl-2,4-pentanediol in the minor groove. *Nucleic Acids Res.*, **29**, 4144–4153.

7. Pohl,F.M. and Jovin,T.M. (1972) Salt-induced co-operative conformational change of a synthetic DNA: equilibrium and kinetic studies with poly(dG–dC). *J. Mol. Biol.*, **67**, 375–396.

8. Tinoco,I.,Jr, Cruz,P., Davis,P., Hall,K., Hardin,C.C., Mathies,R.A., Puglisi,J.D., Trulson,M.A., Johnson,W.C.,Jr and Neilson,T. (1986) Z-RNA: a left-handed double helix. In van Knippenberg,P.H. and Hilbers,C.W. (eds), *Structure and Dynamics of RNA*. Vol. 110. NATO ASI Series A. Plenum Press, New York, NY, pp. 55–69.

9. Barciszewski,J., Jurczak,J., Porowski,S., Specht,T. and Erdmann,V.A. (1999) The role of water structure in conformational changes of nucleic acids in ambient and high-pressure conditions. *Eur. J. Biochem.*, **260**, 293–307.

10. Sugiyama,H., Kawai,K., Matsunaga,A., Fujimoto,K., Saito,I., Robinson,K. and Wang,A.H.-J. (1996) Synthesis, structure and thermodynamic properties of 8-methylguanine-containing oligonucleotides: Z-DNA under physiological salt conditions *Nucleic Acids Res.*, **24**, 1272–1278.

11. Cherrak,I., Mauffret,O., Santamaria,F., Hocquet,A., Ghomi,M., Rayner,B. and Fermandjian,S. (2003) L-Nucleotides and 8-methylguanine of d(C$_1$^{m8}G$_2$C$_3$G$_4$C$_{5L}$G$_{6L}$C$_7$G$_8$C$_9$G$_{10}$)$_2$ act cooperatively to promote a left-handed helix under physiological salt conditions. *Nucleic Acids Res.*, **31**, 6986–6995.

12. Crawford,J.L., Kolpak,F.J., Wang,A.H.-J., Quigley,G.J., van Boom,J.H., van der Marel,G. and Rich.A. (1980) The tetramer d(CpGpCpG) crystallizes as a left-handed double helix. *Proc. Natl Acad. Sci. USA*, **77**, 4016–4020.

13. Uesugi,S., Ohkuko,M., Urata,H., Ikehara,M., Kobayshi,Y. and Kyogoku,Y. (1984) Ribooligonucleotides, r(C-G-C-G) analogues containing 8-substituted guanosine residues, form left-handed duplexes with Z-form-like structure. *J. Am. Chem. Soc.*, **106**, 3675–3676.

14. Nakamura,Y., Fujii,S., Urata,H., Uesugi,S., Ikehara,M. and Tomita,K. (1985) Crystal structure of left-handed RNA tetramer, r(C-br^{8}G)$_2$. *Nucleic Acids Symp. Ser.*, **16**, 29–32.

15. Teng,M.K., Liaw,Y.C., van der Marel,G.A., van Boom,J.H. and Wang,A.H. (1989) Effects of O2' hydroxyl group on Z-DNA conformation: structure of Z-RNA and (*ara*C)-[Z-RNA]. *Biochemistry*, **28**, 4923–4928.

16. Rao,S.N. and Kollman,P.A. (1986) Conformations of the 8-methylated and unmethylated ribohexamer r(CGCGCG)$_2$. *J. Am. Chem. Soc.*, **108**, 3048–3053.

17. Davis,P.W., Adamiak,R.W. and Tinoco,I.,Jr (1990) Z-RNA: the solution NMR structure of r(CGCGCG). *Biopolymers*, **29**, 109–122.

18. Liu,L. F. and Wang,J.C. (1987) Supercoiling of the DNA template during transcription. *Proc. Natl Acad. Sci. USA*, **84**, 7024–7027.

19. Rich,A and Zhang,S (2003) Z-DNA: the long road to biological function. *Nature Rev. Genet.*, **4**, 566–573.

20. Zarling,D.A., Calhoun,C.J., Hardin,C.C. and Zarling,A.H. (1987) Cytoplasmic Z-RNA. *Proc. Natl Acad. Sci. USA*, **84**, 6117–6121.

21. Brown,B.A.,II, Lowenhoupt,K., Wilbert,C.M., Hanlone,E.B. and Rich,A. (2000) The Zα domain of the editing enzyme dsRNA adenosine deaminase binds left-handed Z-RNA as well as Z-DNA. *Proc. Natl Acad. Sci. USA*, **97**, 13532–13536.

22. Brown,B.A.,II, Athanasiadis,A., Hanlon,E.B., Lowenhaupt,K., Wilbert,C.M. Rich,A. (2002) Crystallization of the Zα domain of the human editing enzyme ADAR1 complexes with a DNA–RNA chimeric oligonucleotide in the left-handed Z-conformation. *Acta Crystallogr. D Biol. Crystallogr.*, **58**, 120–123.

23. Schwartz,T., Behlke,J., Lowenhaupt,K., Heinemmann,U. and Rich,A. (2001) Structure of the DLM-1-Z-DNA complex reveals a conserved family of Z-DNA-binding proteins. *Nature Struct. Biol.*, **8**, 761–765.

24. Kim,Y.G., Muralinath,M., Brandt,T., Pearcy,M., Hauns,K., Lowenhaupt,K., Jacobs,B.L. and Rich,A. (2003) Evidence that vaccinia virulence factor E3L binds to Z-DNA *in vivo*: Implications for development of a therapy for poxvirus infection. *Proc. Natl Acad. Sci. USA*, **100**, 6974–6979.

25. Fischer,A., Gdaniec,Z., Biala,E., Lozynski,M., Milecki,J. and Adamiak,R.W. (1996) ^{19}F NMR of RNA. The structural and chemical aspects of 5- fluoro-cytidine and -uridine labelling of oligoribonucleotides. *Nucleosides Nucleotides*, **15**, 477–488.

26. Usman,N., Ogilvie,K.K., Jiang,M.-Y. and Cedergren,R.J. (1987) Automated chemical synthesis of long oligoribonucleotides using 2'-*O*-silylated ribonucleoside 3'-*O*-phosphoramidites on a controlled-pore glass support: synthesis of a 43-nucleotide sequence similar to the 3' half of an *E. coli* formylmethionine tRNA. *J. Am. Chem. Soc.*, **109**, 7845–7854.

27. Biala,E., Milecki,J., Kowalewski,A., Popenda,M., Antkowiak,W.Z. and Adamiak,R.W. (1993) Z-RNA. The synthesis of 2'-*O*-[^{13}C]methyl- and 5-methyl-analogs of ribo-CGCGCG. *Acta Biochim. Pol.*, **40**, 521–530.

28. Piotto,M., Saudek,V. and Sklénar,V. (1992) Gradient-tailored excitation for single-quantum NMR spectroscopy of aqueous solutions. *J. Biomol. NMR*, **6**, 661–665.

29. Sklénar,V., Miyashiro,H., Zon,G. and Bax,A. (1986) Assignment of the ^{31}P and ^{1}H resonances in oligonucleotides by two-dimensional NMR spectroscopy. *FEBS Lett.*, **208**, 94–98.

30. Altona,C. and Sundaralingam,M. (1972) Conformational analysis of the sugar ring in nucleosides and nucleotides. A new description using the concept of pseudorotation. *J. Am. Chem. Soc.*, **94**, 8205–8212.

31. Güntert,P. and Wüthrich,K. (1991) Improved efficiency of protein structure calculations from NMR data using the program DIANA with redundant dihedral angle constraints. *J. Biomol. NMR*, **1**, 447–456.

32. Güntert,P., Mumenthaler,C. and Wüthrich,K. (1997) Torsion angle dynamics for NMR structure calculation with the new program DYANA. *J. Mol. Biol.* **273**, 283–298.

33. Mumenthaler,C., Güntert,P., Braun,W. and Wüthrich,K. (1997) Automated combined assignment of NOESY spectra and three-dimensional protein structure determination. *J. Biomol. NMR*, **10**, 351–362.

34. Parkinson,G., Vojtechovsky,J., Clowney,L., Brünger,A.T. and Berman,H.M. (1996) New parameters for the refinement of nucleic acid-containing structures. *Acta Crystallogr. D Biol. Crystallogr.*, **52**, 57–64.

35. Stallings,S.C. and Moore,P.B. (1997) The structure of an essential splicing element: stem loop IIa from yeast U2 snRNA. *Structure*, **5**, 1173–1185.

36. Lavery,R. and Sklenar,H. (1988) Curves: the definition of generalised helicoidal parameters and of axis curvature for irregular nucleic acids. *J. Biomol. Struct. Dynam.*, **6**, 63–91.

37. Popenda,M., Milecki,J. and Adamiak,R.W. (2004) PDB ID 1T4X, RCSB ID RCSB022316.

38. Wüthrich,K. (1986) *NMR of Proteins and Nucleic Acids*. John Willey & Sons, NY.

39. Feigon,J., Wang,A.H.-J., van der Marel,G.A., van Boom,J.H. and Rich,A. (1984) A one- and two-dimensional NMR study of the B to Z transition of (m^{5}dC-dG)$_3$ in methanolic solution. *Nucleic Acids Res.*, **12**, 1243–1263.

40. Orbons,L.P., van der Marel,G.A., van Boom,J.H. and Altona,C. (1986) The B to Z forms of the d(m^{5}C-G)$_3$ and d(Br^{5}C-G)$_3$ hexamers in solution. A 300 MHz and 500 MHz two- dimensional NMR study. *Eur. J. Biochem.*, **160**, 131–139.

41. Wang,A.H.-J., Quigley,G.J., Kolpak,F.J., van der Marel,G., van Boom,J.H. and Rich,A. (1981) Left-handed double helical DNA. Variations in the backbone conformation. *Science*, **211**, 171–176.

42. Saenger,W. (1984) *Principles of Nucleic Acids Structure*. Springer, Berlin, Heidelberg.

43. Nishimura,Y., Tsuboi,M., Uesugi,S., Ohkubo,M. and Ikehara,M. (1985) Salt induced conformational transition between A and Z forms of r(CGCGCG) as revealed by a Raman spectroscopic study. *Nucleic Acids Symp. Ser.*, **16**, 25–28.

44. Trulson,M.O., Cruz,P., Puglisi,J.D., Tinoco,I.,Jr and Mathies,R.A. (1987) Raman spectroscopic study of left-handed Z-RNA. *Biochemistry*, **26**, 8624–8630.

45. Krzyzaniak,A., Salanski,P., Adamiak,R.W., Jurczak,J. and Barciszewski,J. (1996) Structure and function of nucleic acids under high pressure. In Hayashi,R. and Balny,C. (eds), *High Pressure Bioscience and Biotechnology*. Elsevier Science, Amsterdam, The Netherlands, pp. 189–194.

46. Brown,B.A. and Rich,A. (2001) The left-handed double helical nucleic acids. *Acta Biochim. Pol.*, **48**, 295–312.